Journal of Computer Assisted Tomography
8(4):588–593, August

Measurement of Flow with NMR Imaging Using a Gradient Pulse and Phase Difference Technique

D. J. Bryant, J. A. Payne, D. N. Firmin, and D. B. Longmore

Abstract: A method for determining flow by nuclear magnetic resonance (NMR) imaging is described. A conventional spin-echo imaging sequence is employed with the addition of balanced gradient pulses on either side of the π radiofrequency pulse. Flow velocities in the direction orthogonal to the image plane are determined by the phase shifts in the NMR image. Experimental validation of the technique *in vitro* was achieved with a phantom designed to give a continuous flow of water. The flow rate measured by NMR agreed well with the volume flow rate through the phantom. *In vivo*, NMR flow measurements on the carotid and femoral arteries of two volunteers were compared with Doppler ultrasound results. Velocity measurements were in general agreement. Rapid changes in flow are difficult to follow with the NMR method unless particular care is taken in gradient profile design. The technique can readily be used in existing NMR imaging machines and may have a useful clinical role. **Index Terms:** Blood, flow dynamics—Nuclear magnetic resonance, techniques—Nuclear magnetic resonance.

The appearance of flowing blood with nuclear magnetic resonance (NMR) can vary widely with different imaging techniques. Many of these differences are due to changes in the degree of saturation of blood in the imaging plane caused by the flow of fully magnetised blood into the slice.

Methods for quantifying flow velocity that measure amplitude of transverse magnetisation usually require a knowledge of the T1 and T2 of the flowing material or rely on a comparison of degrees of saturation between static and flowing components (1,2). These techniques may require fast pulse repetition rates, which distort the selected slice shape.

An alternative technique is described in which field gradients are applied briefly in the z direction in such a way that flow in that direction produces a phase shift in the transverse component of the magnetisation of the flowing material. Such phase shifts are observable and depend on the flow velocity. The field gradient pulses can be arranged so that static material in the slice acquires no shift in phase. Shifts of phase from zero indicate material that has moved during the time between the two gradient pulses. This method avoids the use of fast pulse repetition rates and may be used within the framework of existing spin-echo imaging sequences. The technique was assessed *in vitro* using a simple flow phantom and *in vivo* on the carotid and femoral arteries of two human volunteers.

From the Hirst Research Centre, Picker International, Wembley, Middlesex (D. J. Bryant and J. A. Payne), and The National Heart Hospital, London (D. N. Firmin and D. B. Longmore), England. Address correspondence and reprint requests to Dr. Bryant at Hirst Research Centre, Picker International, East Lane, Wembley, Middlesex HA9 7PP, England.

THEORY

The transverse component of magnetisation ($M_{x'y'}$) (3) following a $\pi/2$ pulse is phase shifted when subjected to a magnetic field gradient $G(t)$ for a short time period δ by an amount ϕ given by

$$\phi = \gamma \int_{t}^{t+\delta} G(t) \cdot r(t)\, dt \qquad (1)$$

where γ is the magnetogyric ratio of the nucleus under observation and $r(t)$ is the position vector that, for flowing material, changes with time. To measure flow in the longitudinal direction, the gradient G should lie in the z direction, so that the static field B_0 is stronger above the imaged slice and weaker below it.

The flow-measuring technique described herein utilizes the spin-echo imaging sequence with two

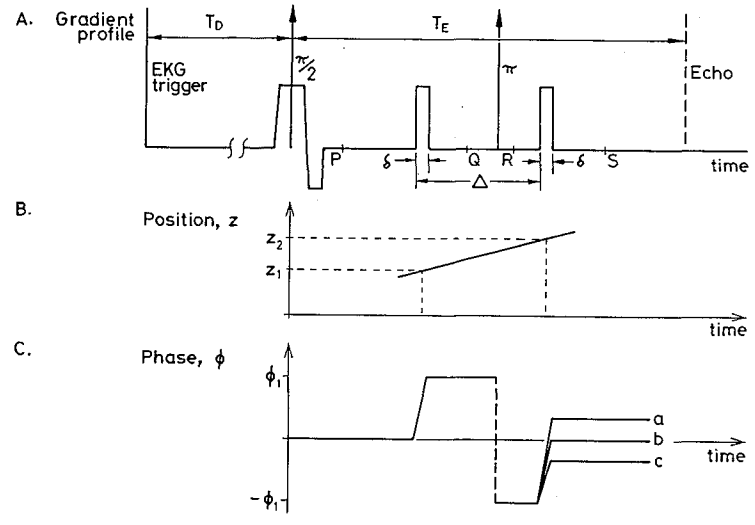

FIG. 1. Flow velocity measurement. **a:** Electrocardiograph-triggered spin-echo sequence. Gating delay (TD) is the delay between EKG R wave and the π radiofrequency (RF) pulse. A slice select gradient is applied at the same time as the $\pi/2$ RF pulse. Two short gradient pulses of duration δ and separated by time Δ, during which the π RF pulse is applied, phase encode the flowing nuclei. The magnetisation for static material refocusses at time TE after the $\pi/2$ RF pulse. Letters P, Q, R, and S denote times used in Fig. 2. **b:** Linear change in z coordinate for nuclei moving at constant velocity. At the first gradient pulse the position of the flowing nuclei is z_1; at the second gradient pulse their position has shifted to z_2. **c:** Changes in phase of material in the selected slice. At the first gradient pulse a change in phase of ϕ_1 occurs. The π RF pulse reverses this to $-\phi_1$ and a second phase shift occurs at the second gradient pulse. Nuclei moving to higher z have a net phase shift that is positive (a); static nuclei have no shift (b); and nuclei moving to lower z have a net negative phase shift (c).

such brief applications, or pulses, of a z gradient: one before the π radiofrequency (RF) pulse, which is used to form the spin echo at time TE, and one after (Fig. 1a).

Assuming a constant velocity in the z direction, the change in position of a particular flowing nucleus is shown in Fig. 1b and the corresponding change in phase is shown in Fig. 1c.

We assume that δ is short enough so that negligible flow occurs during the application of each pulse and that the gradient is constant during this period. The first phase shift ϕ_1 ($\gamma G\delta z_1$) is reversed by the π RF pulse before the second phase shift ϕ_2 ($\gamma G\delta z_2$) occurs. Between the two gradient pulses (separated by the time Δ) the nuclei move along the z axis by a distance $v\Delta$. The overall phase shift for flowing material is given by

$$\phi = \gamma G\delta\Delta v \text{ (radians)} \qquad (2)$$

The phase shift is thus directly proportional to velocity. The two gradient pulses are adjusted experimentally to ensure that static material in the imaging plane acquires no phase shift.

Phase angles can only be defined unambiguously in the range $-\pi$ to π. Phase shifts outside this range may simulate motion in the reverse direction. This may be readily recognised if velocities are such that the phase shift is not too far in excess of $\pm\pi$ and the vessel is reasonably large. Where the ambiguity is not resolved the amplitude (G), width (δ), or separation (Δ) may be adjusted to reduce the phase shift.

In general the NMR image represents the transverse magnetisation at some defined point in a sequence of RF pulses. For the usual sequences employed in NMR imaging (partial saturation, spin-echo, and inversion-recovery), this magnetisation lies along the y′ axis of the rotating frame, and image intensity represents the amplitude of this component. In mathematical terms the output of the

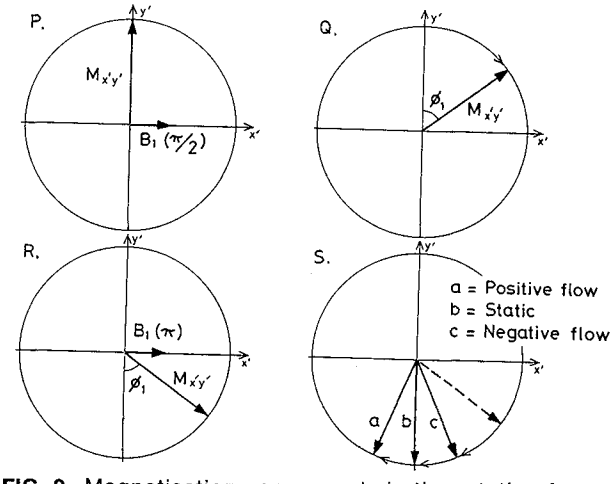

FIG. 2. Magnetisation components in the rotating frame during the velocity-determining gradient profile. Letters P, Q, R, and S are successive points in the spin-echo sequence shown in Fig. 1. P, The slice selective $\pi/2$ radiofrequency pulse (B_1) applied along the x′ axis of the rotating frame rotates in-slice magnetisation $M_{x'y'}$ along the y' axis. Q, Following the first gradient pulse, transverse magnetisation components $M_{x'y'}$ accumulate a phase shift ϕ_1 dependent on the position of nuclei at the time of this pulse. R, The nonselective π RF pulse (B_1) inverts the angle ϕ_1 by changing the sign of the component of magnetisation along the y' axis. S, The magnetisation vector (position prior to the second gradient pulse is shown in a dashed line) is further rotated by this gradient pulse. Material moving to higher z precesses beyond the $-y'$ direction (a); static material is aligned along the $-y'$ axis (b); and nuclei moving to lower z are aligned in the direction shown by (c).

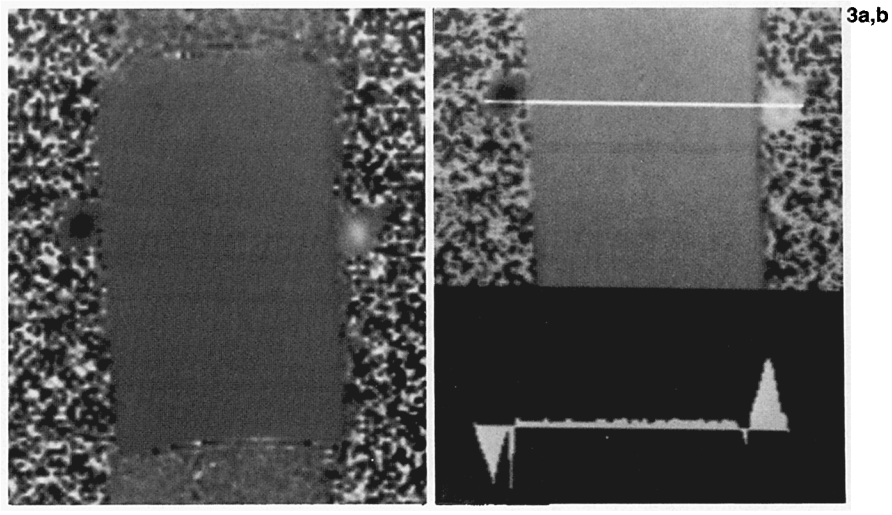

FIG. 3. Phase map for flow phantom. Phase shifts in the range $-\pi$ to π are displayed in a gray scale **(a)**. The static material in the central bottle appears as midgray. Variations in image intensity across the tube containing flowing water are emphasised by the histogram of phase shifts across the phantom **(b)**. The mean flow velocity in this case was 0.94 cm/s.

image reconstruction processing is real. The transverse components of magnetisation are illustrated in Fig. 2 at four instants during the velocity-measuring gradient profile (Fig. 1a). Static material is unaffected by the gradient pulses, and its transverse magnetisation remains aligned along y'. Magnetisation for flowing material (Fig. 2—S) is oriented in a more general sense in the $x'y'$ plane and is described by an amplitude and a phase angle. The phase shifts of the image are displayed in a phase map and indicate regions where flow of nuclei has occurred.

MATERIALS AND METHODS

In vitro and *in vivo* experiments were done at the Royal Postgraduate Medical School, Hammersmith Hospital, using an NMR imaging system described previously (3).

The balanced pair of z-gradient pulses were used in conjunction with TE = 40 ms spin-echo imaging sequence.

In all cases two averages of each data line were taken with a repetition time of 540 ms and the data reconstructed by two-dimensional Fourier transformation to give a 256 × 256 matrix image. The image displayed the phase shifts occurring in the magnetisation components in the image plane. These phase shifts are in the range $-\pi$ to π radians and are shown in a gray scale; static material with zero phase shift is therefore displayed as midgray. In regions where no signal was received, a noisy area was seen. This noise is the calculation of the phase angle from the components $M_{x'}$ and $M_{y'}$ of transverse magnetisation and does not represent the actual noise in the system.

Phantom Studies

The flow phantom consisted of a central static bottle with 1.25 cm internal diameter tubes on either side carrying a 1 mM copper sulphate solution. The flow was nonpulsatile and the pump speed was calibrated in order that known volume flow rates could be obtained. Mean flow velocities of up to 40 cm/s

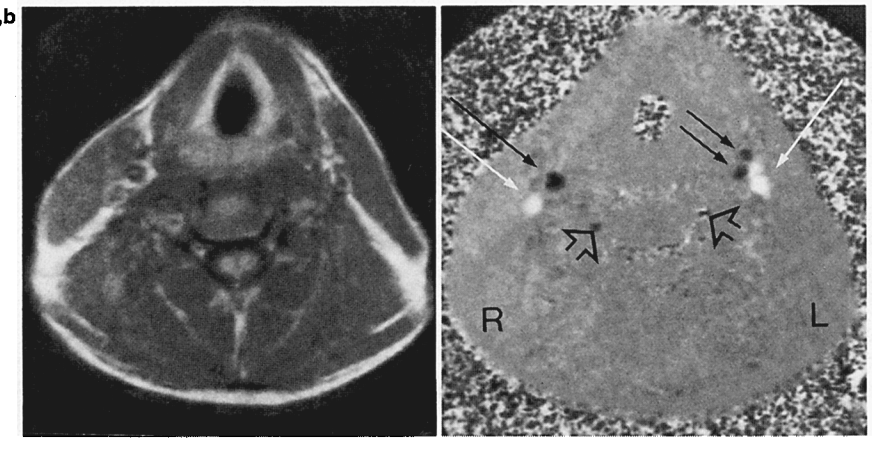

FIG. 4. Normal anatomy for an $SE_{540/40}$ sequence **(a)** and phase map **(b)** at the same level of the neck 50 ms following the R wave. Blood flow is seen in right common carotid (long black arrow) and the left internal and external carotid arteries (short black arrows) as well as the vertebral arteries (open black arrows). Venous flow is seen in the internal jugular veins (long white arrows).

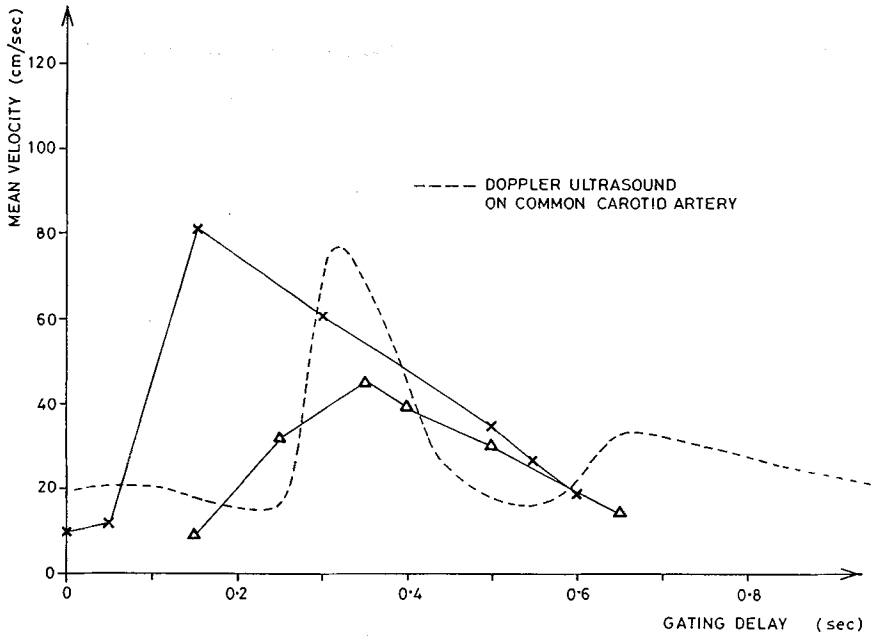

FIG. 5. Mean flow velocity through the cardiac cycle in the internal carotid artery. The x and △ indicate results on two occasions. For comparison, Doppler ultrasound measurements on the common carotid artery are overlaid.

were used with this phantom and a comparison made with the peak flow velocities determined by the NMR method described above.

Volunteer Studies

The experiments were done with the approval of the Research Ethics Committee of the Royal Postgraduate Medical School, Hammersmith Hospital. Electrocardiographic (EKG) gating was employed to synchronize data acquisition with the R wave. Sequences included a delay period between the R wave of the EKG and the $\pi/2$ pulse of the NMR sequence (Fig. 1a). Phase maps were constructed at 50 ms intervals throughout the cardiac cycle for selected levels in the neck and the proximal thigh. The pulsed Doppler ultrasound studies were performed with an ATL scanner at St. Mary's Hospital.

RESULTS

Phantom Studies

A phase map for the flow phantom is shown in Fig. 3. The static water of the central bottle shows the midgray expected for static material. The deviations from zero phase shift in this region of the phantom were within 10% and this was taken to be the accuracy of the phase determination. Phase shifts in the tubes had the same magnitude but opposite direction (Fig. 3b). The difference in direction is indicated by the shading from black to white. Shading across the diameter of the flow tubes indicates the velocity profiles.

The comparison of peak flow velocities agreed well with those expected for 20 calibrated volume flow rates. In each case the agreement was within the 10% noise level for mean velocities up to the

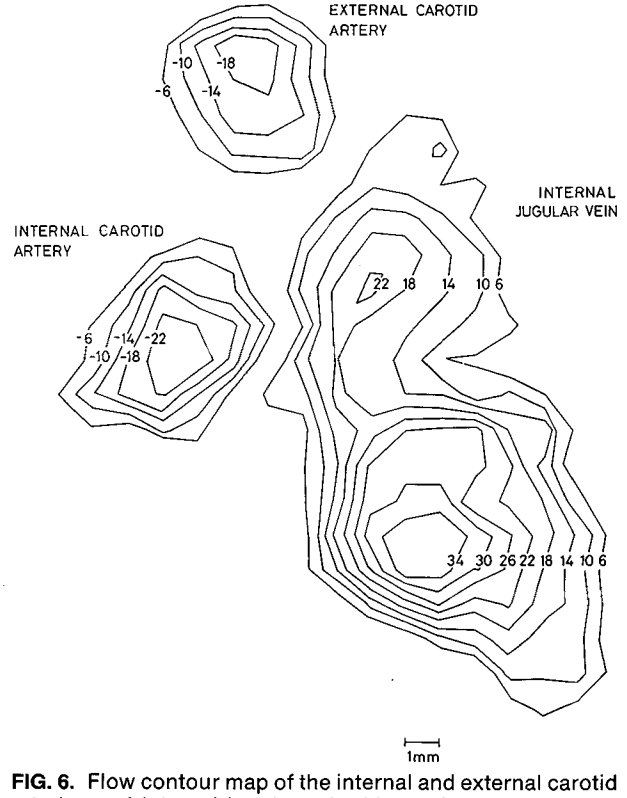

FIG. 6. Flow contour map of the internal and external carotid arteries and internal jugular vein. Lines of equal phase are shown as a contour map. The positive and negative shifts are interpreted as velocities (cm/s). An integration across the cross-sectional area of the vessels gives the volume flow rate.

7a,b

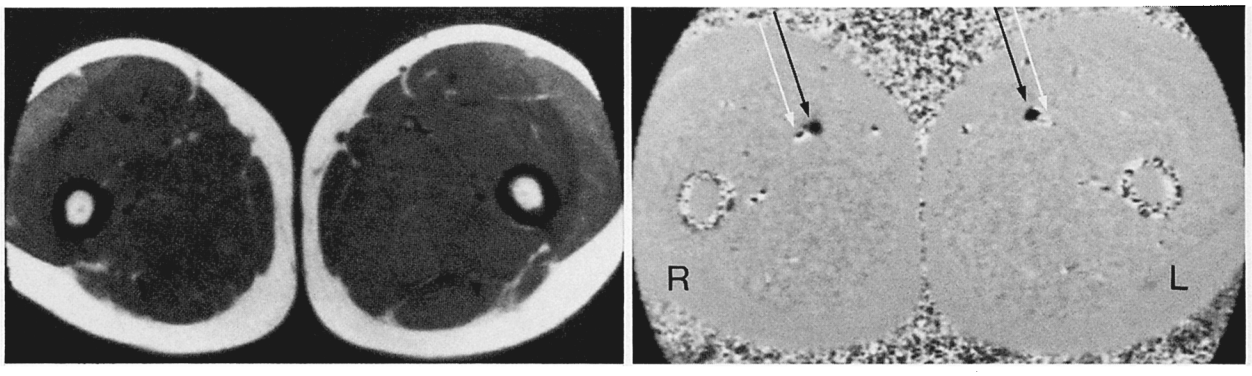

FIG. 7. Normal anatomy for an $SE_{540/40}$ sequence **(a)** and phase map **(b)** at the same level of the proximal thigh 150 ms following the R wave. The femoral arteries are black (black arrows) and the femoral veins are light (white arrows). Static tissue is midgray.

maximum of 40 cm/s. This comparison is quicker and simpler than a determination of the volume flow rate from the NMR data, which would also require an accurate measurement of the cross-sectional area. For simple Newtonian fluids in which the flow is laminar, the peak velocity is twice the mean flow through the section of the pipe.

Volunteer Studies

Flowing blood within the external and internal carotid arteries and internal jugular veins at the level of the bifurcation is clearly shown in Fig. 4. Fig. 5 shows the mean velocity integrated across the cross-sectional area of the internal carotid artery for different values of the gating delay. Superimposed on these data is the pulsed Doppler ultrasound flow velocity for the common carotid artery at a point approximately 2 cm below the bifurcation. The internal and external carotid arteries and jugular vein shown on the right side of the neck in Fig. 4 have been interpolated onto a finer matrix. The result is shown in Fig. 6 where Eq. 2 has been used with the known experimental values for G, δ, and Δ to determine the flow velocities, and contours of equal velocity are shown.

The image pixel size was determined by imaging a bottle of known dimensions. Volume flow rates were then calculated from the cross-sectional area within each contour of Fig. 6. At this point of the cardiac cycle, 50 ms following the R wave of the EKG, the volume flow rate through the internal jugular veins was calculated to be 16 ml/s. The arterial flow was somewhat lower: 3 ml/s through the external carotid and 4 ml/s^{-1} through the internal carotid artery. The errors in these numbers will exceed the 10% of the phase determination due to the indeterminancies in the exact cross-sectional area.

Figure 7 is a scan through the proximal thigh including the femoral artery and vein. At this level, with the imaging gradients employed, these vessels were no more than 4 pixels in diameter and the anatomy of the region with the vein partially wrapped round the artery as venae comitantes makes accurate velocity determination difficult. In the clearest images preliminary results agreed with the pulsed Doppler ultrasound, the NMR giving a peak in flow velocity 200 ms after the R wave as in the internal carotid artery shown in Fig. 4. The results are not presented in more detail here.

DISCUSSION

The technique provides a useful method for measuring flow *in vitro* and blood flow *in vivo*. The preliminary results show general agreement with phantom and Doppler flow studies.

The spin-echo technique has been used for the investigation of translation of nuclei for many years (4,5). In particular the pulsed gradient method (6) has been employed to study diffusion. Diffusion differs from flow in that its incoherence introduces a reduction of amplitude of the spin echo as a result of incomplete refocussing of the transverse magnetisation components. Flow does not introduce incoherence into the transverse magnetisation and observable phase shifts may therefore be encoded into flowing material providing the basis for the technique described above. The method records the position of the nuclei at the times of the two gradient pulses and the velocity is determined from the distance traversed between these pulses giving an average velocity. Rapid changes in velocity are best followed with gradient pulses with a small separation.

In vivo NMR flow measurement may have useful clinical applications, particularly in those situations in which blood vessels are inaccessible to Doppler flow techniques.

Acknowledgment: We are grateful to the staff of the Department of Health and Social Security for their help and encouragement with this study. We would also like

to thank Dr. G. M. Bydder for helpful comments and advice during the course of this work.

REFERENCES

1. Singer JR. NMR diffusion and flow measurement and an introduction to spin phase graphing. *J Phys* [*E*] 1978;11: 281–91.
2. Singer JR, Crooks LE. Nuclear magnetic resonance blood flow measurements in the human brain. *Science* 1983;221:654–6.
3. Young IR, Bailes DR, Burl M, et al. Initial clinical evaluation of a whole body nuclear magnetic resonance (NMR) tomograph. *J Comput Assist Tomogr* 1982;6:1–18.
4. Hahn EL. Spin echoes. *Phys Rev* 1950;80:580–94.
5. Carr HY, Purcell EM. Effects of diffusion on free precession in nuclear magnetic resonance experiments. *Phys Rev* 1958;94:630–8.
6. Stejskal EO, Tanner JE. Spin diffusion measurements: spin echoes in the presence of a time-dependent field gradient. *J Chem Phys* 1965;42:288–92.